Multiscale and Layer-Stripping Wave-Equation Dispersion Inversion of Rayleigh Waves

Zhaolun Liu[1,2] *and Lianjie Huang*[1]
[1]*Los Alamos National Laboratory, Geophysics Group, MS D452, Los Alamos, NM 87545, USA*
[2]*King Abdullah University of Science and Technology (KAUST), Division of Physical Science and Engineering, Thuwal, Saudi Arabia*

SUMMARY

Rayleigh-wave inversion could converge to a local minimum of its objective function for a complex subsurface model. We develop a multiscale strategy and a layer-stripping method to alleviate the local minimum problem of wave-equation dispersion inversion of Rayleigh waves, and improve the inversion robustness. We first invert the high-frequency and near-offset data for the shallow S-velocity model, and gradually incorporate the lower-frequency components of data with longer offsets to reconstruct the deeper regions of the model. We demonstrate the efficacy of this multiscale and layer-stripping method using synthetic and field Rayleigh-wave data.

INTRODUCTION

Wave-equation dispersion inversion (WD) of Rayleigh waves uses solutions to the 2D or 3D elastic-wave equation to invert the dispersion curves of surface waves for the S-velocity model (Li and Schuster, 2016; Li et al., 2016, 2017a,b,c; Liu et al., 2017). The advantage of WD over the traditional dispersion inversion method (Haskell, 1953; Xia et al., 1999, 2002; Park et al., 1999) is that WD does not assume a layered velocity model and is valid when there are strong lateral gradients in the S-velocity model. The WD method also enjoys robust convergence because the skeletonized data, namely the dispersion curves, are simpler than a trace with many dispersive arrivals. Such traces are used in full waveform inversion (FWI) (Groos et al., 2014; Pérez Solano et al., 2014; Dou and Ajo-Franklin, 2014; Groos et al., 2017).

The iterative WD method can suffer from the local minimum problem when inverting seismic data from complex Earth models. One method to tackle this problem is the multiscale method (Masoni et al., 2016). For body waves, the low-to-high frequency content of data is first used to update the large-scale velocity structure and then the more detailed features of the velocity model are reconstructed (Sirgue and Pratt, 2004; Bunks et al., 1995). However, a high-to-low frequency strategy for surface waves is needed because the frequency content of surface waves is directly related to their penetration depth: higher-frequency and shorter-wavelength surface waves sample the top layers of a medium, while lower-frequency and longer-wavelength surface waves sample deeper subsurface regions (Masoni et al., 2016).

The WD method needs to determine the offset range (denoted as R) starting from the near offset for retrieving the dispersion curves of the data using F-K or Radon transforms. A narrow range of offsets corresponding to a small R is not adequate for accurate retrieval of the low-frequency component of dispersion curves (indicated in Figs. 2.3-8 of Yilmaz (2015)), but can provide high lateral resolution in the tomographic image. Conversely, a wide range of offsets is adequate for accurately retrieving the low-frequency dispersion curves but the penalty is that it only provides a low-wavenumber estimate of the velocity model. As a rule of thumb, we choose R to be about three or four times greater than the depth of interest to make sure that WD has enough penetration depth and lateral resolution. However, a fixed value of R would result in a loss of either the low-frequency information in the dispersion curves or the lateral resolution of the inverted S-velocity model. Thus, an iterative small-to-large offset range strategy is needed to obtain both high lateral resolution and low-frequency information.

In this paper, we first use the high-frequency surface-wave data with a small-offset range to update the shallow velocity model, and then use the low-frequency surface-wave data with a large-offset range to update the deeper regions of the velocity model. We employ a layer-stripping method (Shi et al., 2015; Masoni et al., 2016) to reconstruct the velocity model from the shallow to deep regions. The layer-stripping method assumes that all layers above a given layer have been inverted using the near-offset and high-frequency surface-wave data. We use the far-offset and low-frequency data, to invert for the velocity model of the deep layers. This procedure is repeated until the entire volume of interest is reconstructed.

After the introduction, we describe the theory of WD and the workflow for the layer-stripping approach. Numerical tests on synthetic and field surface-wave data are presented in the third section to demonstrate the improvement of the method, followed by the conclusions.

THEORY

The WD method inverts for the S-wave velocity model to minimize the dispersion objective function

$$\varepsilon = \frac{1}{2}\sum_{\omega}\sum_{\theta}\overbrace{[\kappa(\theta,\omega)_{pre}-\kappa(\theta,\omega)_{obs}]}^{residual=\Delta\kappa(\theta,\omega)}{}^2, \qquad (1)$$

where $\kappa(\omega,\theta)_{pre}$ represents the predicted dispersion curve picked from the simulated spectrum along the azimuth angle θ, and $\kappa(\omega,\theta)_{obs}$ describes the observed dispersion curve obtained from the recorded spectrum along the azimuth θ. In the 2D case, the azimuth angles have only two values: 0° and 180°, corresponding to the left and right directions, respectively. The gradient $\gamma(\mathbf{x})$ of ε with respect to the S-wave velocity $v_s(\mathbf{x})$ is given in (Liu et al., 2017), which is computed using a weighted zero-lag correlation between the source and backward-extrapolated receiver wavefields.

10.1190/segam2018-2997500.1

The optimal S-wave velocity model $v_s(\mathbf{x})$ is obtained using the steepest-descent formula (Nocedal and Wright, 2006)

$$v_s(\mathbf{x})^{(k+1)} = v_s(\mathbf{x})^{(k)} - \alpha\gamma(\mathbf{x}), \tag{2}$$

where α is the step length and the superscript (k) denotes the k^{th} iteration. We use a preconditioned conjugate gradient method to update the S-wave velocity model.

For layer-stripping WD (LSWD), we use the high-frequency data with a small R to first update the shallow velocity model. Then we assume this shallow velocity model is known and use the low-frequency data with a large R to update the deeper regions of the velocity model. For a given frequency band, according to the dispersion curves, we estimate an average wavelength

$$\lambda = 1/\kappa,$$

where κ is the average wavenumber. The penetration depth z is estimated as half of the wavelength λ, and the maximum offset R is estimated as three or four wavelengths.

Workflow

1. Determine the frequency range of observed data. Divide the frequency range into several frequency bands for each LSWD step. The frequency-band selection rule is the following:
2. Retrieve the dispersion curves from the whole common-shot gather (CSG) and estimate the range of the average wavenumber k for each frequency band.
3. For a given frequency band, determine the maximum offset R according to the maximum wavelength λ calculated from the range of k values and estimate the observed dispersion curves from traces within the maximum offset R for each CSG.
4. Calculate the gradient and only the region within a depth window is used to update the S-velocity model. The depth window can be estimated from half of the wavelength range.
5. Use the updated S-velocity model as the initial model to perform WD for the next frequency band.
6. Repeat the last three steps for all frequency bands.

NUMERICAL RESULTS

Synthetic Model

We first use a synthetic model displayed in Fig. 1a to validate the effectiveness of LSWD. The model is modified from Pérez Solano et al. (2014) (Fig. 6d) and used by Masoni et al. (2016) (Fig. 4). Only the S-wave velocity model is inverted. We use the actual P-wave velocity model for modeling predicted surface waves. The source wavelet is a Ricker wavelet with a center frequency of 40 Hz, which is assumed to be known during inversion. The P-wave velocity v_p is calculated from the S-wave velocity v_s using the relation $v_p = 2v_s$, with a homogeneous density model of 1000 kg/m^3. The fundamental dispersion curves from each common-shot gather are used for inversion along the azimuth angles of 0° (toward the right-hand side) and 180° (toward the left-hand side).

A total of 40 CSGs are simulated for vertical sources located at $z = 0.2$ m below the free surface with a spatial interval of 1.5 m. Each CSG has 150 vertical-component receivers at $z = 0.2$ m below the surface with a spatial interval of 0.2 m. The initial S-velocity model used is a model with a linear gradient in depth (Fig. 1b).

We first apply the single-scale WD to the data by setting the receiver spread length R as 8 m and 20 m, respectively. The inverted S-velocity tomograms with a maximum offset of $R =$ 8 m and R=20 m are shown in Figs. 1c and 1d, respectively. The high-velocity anomalies are not detected in the inverted tomograms of these two tests. This suggests that WD converges to a local minimum because of the shallow low-velocity zone. To alleviate this problem, we use the layer-stripping WD method.

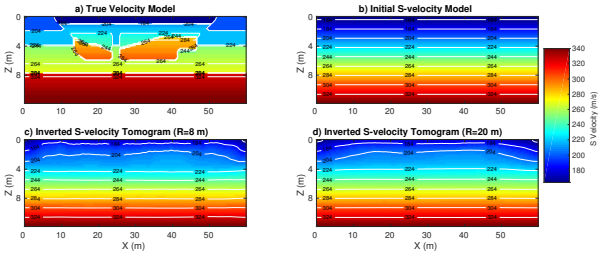

Figure 1: The true (a) and initial (b) S-velocity models together with the inverted S-velocity model using WD with the maximum offsets of $R = 8$ m (c) and (d) $R = 20$ m (d).

We then apply layer-stripping WD to the same data as above, where eleven frequency bands are chosen for inversion. Larger frequency windows are selected for high-frequency bands because of the small amplitude of the frequency spectrum of surface wave data. The ranges of the eleven frequency bands and the wavelength range corresponding to each frequency band are listed in Table 1. The maximum offset R is calculated using

$$R \approx 3.5 * \lambda_{max} \tag{3}$$

where λ_{max} is the maximum wavelength. The misfit-change column shows the normalized misfit change after 10 iterations. The updated depth window for each frequency band is determined using half of the wavelength. A taper is used at the top and bottom boundaries of a depth window. The updated velocity models for all eleven steps are shown in Figs. 2 and 3, where the black dashed lines indicate the location of the high-velocity anomalies. We can see that the deeper region of the model is gradually updated step by step. The vertical-velocity profiles at $X = 20$ m and $X = 38$ m extracted from the inverted tomogram with layer stripping (red lines) are shown in Fig. 4. They show better agreement with the true ones (blue lines) than those extracted from the tomogram without layer stripping (magenta lines). The results demonstrate that LSWD can mitigate the local minimum problem of WD for this model caused by the low-velocity layer in the shallow region.

Surface Seismic Data from the Blue Mountain Geothermal Site

Seven 2D lines of surface seismic data were acquired at the Blue Mountain geothermal site in Nevada, USA, using dynamite sources. We use one 2D line of data for our study. The

10.1190/segam2018-2997500.1

Table 1: Eleven frequency bands used for LSWD, where the wavelength λ is estimated from the dispersion curves; the maximum offset are determined using $R = 3.5\lambda_{max}$; the depth range is calculated using half of the wavelength range with a taper of 0.2 m at both ends.

No.	Freq. Band (Hz)	λ Range (m)	Max. Offset (m)	Depth Range (m)	Misfit Change
1	90-110	1.4-1.9	7	0-1.0	1→0.148
2	70-90	1.9-2.4	9	1-1.4	1→0.4
3	60-70	2.4-2.9	11	1.4-1.6	1→0.1
4	50-60	2.9-3.6	13	1.6-2.0	1→0.13
5	40-50	3.6-4.7	17	2.0-2.6	1→0.125
6	35-40	4.7-5.45	21	2.6-3.0	1→0.1
7	30-35	5.45-6.6	24	3.0-3.6	1→0.17
8	25-30	6.6-8.26	30	3.6-4.2	1→0.25
9	20-25	8.26-10.87	37	4.2-5.2	1→0.35
10	15-20	10.87-15.74	46	5.2-7.4	1→0.7
11	10-15	15.74-33	60	7.4-12	1→0.72

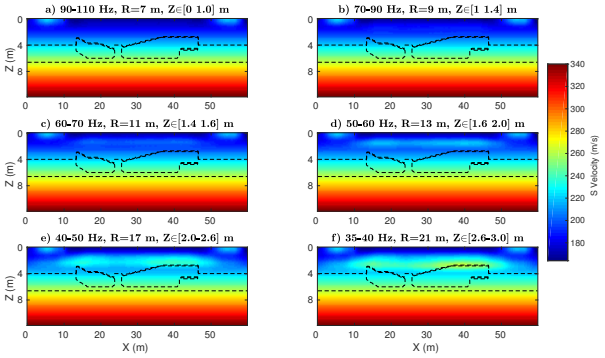

Figure 2: The inverted S-velocity tomograms for steps 1 to 6 (Table 1).

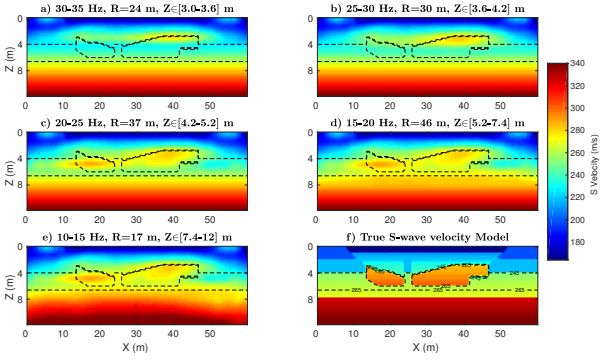

Figure 3: (a)-(e): The inverted S-velocity tomograms for steps 7 to 11 (Table 1). (f): The true S-velocity model.

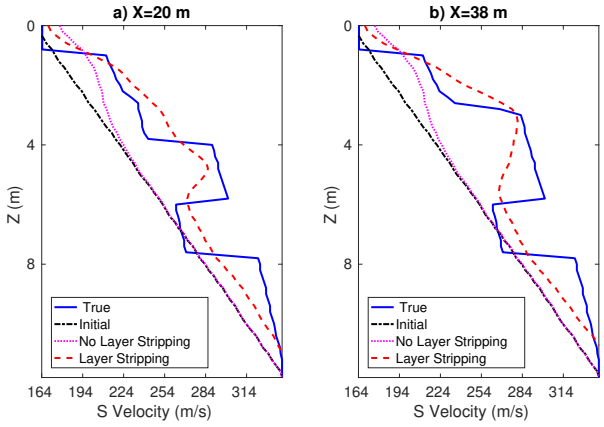

Figure 4: The vertical-velocity profiles at (a) $X = 20$ m and (b) $X = 38$ m for the true model (blue lines), the initial model (black lines), the inverted tomograms with (red lines) and without (magenta lines) layer stripping.

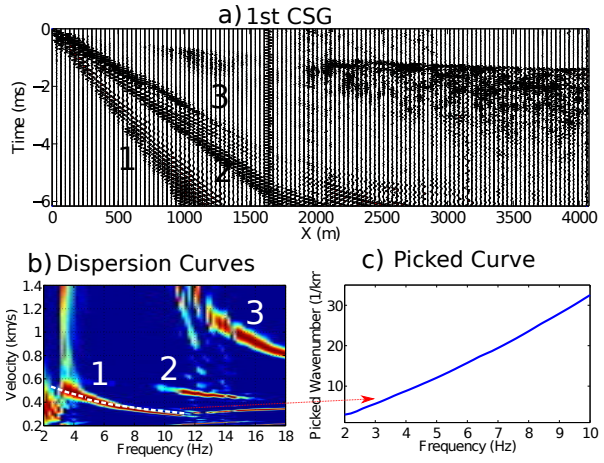

Figure 5: (a) The first CSG of a 2D line of seismic data from the Blue Mountain geothermal field; (b) dispersion images for the first CSG with the maximum offset R=1000 m; (c) picked fundamental mode dispersion curve for the first CSG.

10.1190/segam2018-2997500.1

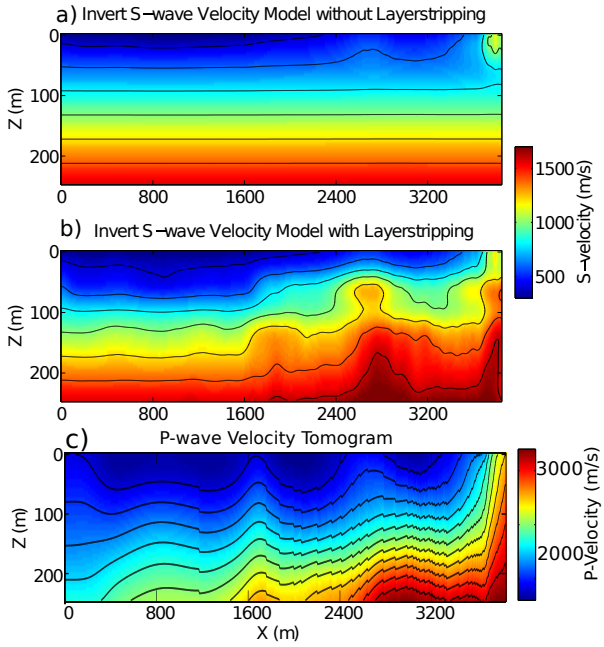

Figure 6: (a) The inverted S-velocity model obtained using WD without layer stripping; (b) the inverted S-velocity model obtained using layer-stripping WD; (c) the P-wave velocity tomogram.

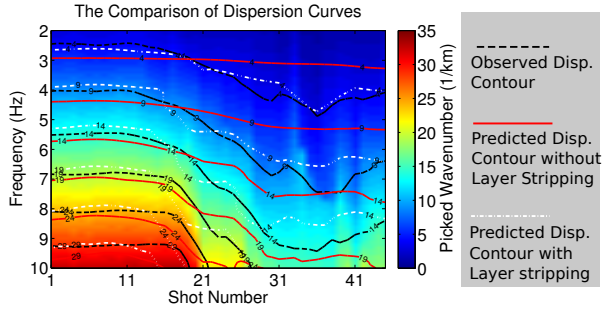

Figure 7: The observed dispersion curves (azimuth angle $\theta = 0^\circ$ and $R = 1000$ m) retrieved for all CSGs of a 2D line data from the Blue Mountain geothermal field, where the black dashed lines, the white dash-dot lines and the red lines represent the contours of the observed dispersion curves, the inverted dispersion curves without layer stripping and the inverted dispersion curves with layer stripping, respectively.

line consists of 121 receivers with an interval of 33.5 m, and 59 dynamite sources with an interval of 67 m. One of the CSGs is shown in Fig. 5a, which clearly shows three modes of surface waves. These three modes are also shown in the dispersion images (Fig. 5b) calculated using a Radon transform with the maximum offset R =1000 m. We pick only the dispersion curves of the fundamental mode (Fig. 5c). The initial S-velocity model used for WD is a linear gradient in depth.

We use three frequency bands for LSWD: (a) 6-10 Hz, (b) 4-8 Hz and (c) 2-6 Hz. The corresponding depth windows are 0-45 m, 45-100 m and 100-250 m. The comparison of the inverted S-velocity tomograms with and without using the layer stripping approach are shown in Fig. 6a and b. It can been seen that the deeper regions are accurately updated using layer-stripping WD. The inverted S-velocity tomogram is also consistent with the P-wave tomogram shown in Fig. 6c. The predicted dispersion contours with and without layer stripping are displayed in Fig. 7. The dispersion contours from low-frequency components and the CSGs No.21-41 correlate better with the observed ones.

CONCLUSIONS

We have developed a multiscale and layer-stripping wave-equation dispersion inversion method for Rayleigh waves to improve the inversion robustness. In this method, the high-frequency and near-offset data are first used to invert for the shallow S-velocity model, and the lower-frequency data with longer offsets are gradually incorporated to invert for the deeper regions of the model. Our results of synthetic surface seismic data demonstrate that layer-stripping wave-equation dispersion inversion provides better depth penetration and higher lateral resolution than the traditional wave-equation dispersion inversion without layer stripping. Numerical results of both synthetic and field seismic data show that the wave-equation dispersion inversion can suffer from the local minimum problem when inverting seismic data from a complex Earth model. Our multiscale and layer-stripping wave-equation dispersion inversion can mitigate the local minimum problem and enhance the convergence of wave-equation dispersion inversion. The major challenge is that it is not easy to determine the correct relationship between the frequency bands and the depth windows because this relationship depends on the unknown velocity model.

ACKNOWLEDGMENTS

This work was supported by U.S. Department of Energy through contract DE-AC52-06NA25396 to Los Alamos National Laboratory (LANL). Zhaolun Liu would like to thank King Abdullah University of Science and Technology (KAUST) for funding his graduate studies. The computation was performed using super-computers of LANL's Institutional Computing Program. Additional computational resources were made available through the KAUST Supercomputing Laboratory (KSL).

10.1190/segam2018-2997500.1

REFERENCES

Bunks, C., F. M. Saleck, S. Zaleski, and G. Chavent, 1995, Multiscale seismic waveform inversion: Geophysics, **60**, 1457–1473, https://doi.org/10.1190/1.1443880.

Dou, S., and J. B. Ajo-Franklin, 2014, Full-wavefield inversion of surface waves for mapping embedded low-velocity zones in permafrost: Geophysics, **79**, no. 6, EN107–EN124, https://doi.org/10.1190/geo2013-0427.1.

Groos, L., M. Schäfer, T. Forbriger, and T. Bohlen, 2014, The role of attenuation in 2D full-waveform inversion of shallow-seismic body and Rayleigh waves: Geophysics, **79**, no. 6, R247–R261, https://doi.org/10.1190/geo2013-0462.1.

Groos, L., M. Schäfer, T. Forbriger, and T. Bohlen, 2017, Application of a complete workflow for 2D elastic full-waveform inversion to recorded shallow-seismic Rayleigh waves: Geophysics, **82**, no. 2, R109–R117, https://doi.org/10.1190/geo2016-0284.1.

Haskell, N. A., 1953, The dispersion of surface waves on multilayered media: Bulletin of the Seismological Society of America, **43**, 17–34.

Li, J., G. Dutta, and G. Schuster, 2017a, Wave-equation Q_S inversion of skeletonized surface waves: Geophysical Journal International, **209**, 979–991, https://doi.org/10.1093/gji/ggx051.

Li, J., G. Dutta, and G. Schuster, 2017b, Skeletonized wave-equation Qs tomography using surface waves: 87th Annual International Meeting, SEG, Expanded Abstracts, 2726–2731, https://doi.org/10.1190/segam2017-17784736.1.

Li, J., Z. Feng, and G. Schuster, 2017c, Wave-equation dispersion inversion: Geophysical Journal International, **208**, 1567–1578, https://doi.org/10.1093/gji/ggw465.

Li, J., and G. Schuster, 2016, Skeletonized wave equation of surface wave dispersion inversion: 86th Annual International Meeting, SEG, Expanded Abstracts, 3630–3635, https://doi.org/10.1190/segam2016-13770057.1.

Li, J., G. Schuster, F.-C. Lin, and A. Alam, 2017d, Wave-equation dispersion inversion of surface waves recorded on irregular topography: 87th Annual International Meeting, SEG, Expanded Abstracts, 2621–2626, https://doi.org/10.1190/segam2017-17663038.1.

Liu, Z., J. Li, and G. Schuster, 2017, 3D wave-equation dispersion inversion of surface waves: SEG 2017 Workshop: Full-waveform Inversion and Beyond, 22–26, https://doi.org/10.1190/FWI2017-007.

Masoni, I., J.-L. Boelle, R. Brossier, and J. Virieux, 2016, Layer stripping FWI for surface waves: 86th Annual International Meeting, SEG, Expanded Abstracts, 1369–1373, https://doi.org/10.1190/segam2016-13859781.1.

Nocedal, J., and S. Wright, 2006, Numerical optimization: Springer Science & Business Media.

Park, C. B., R. D. Miller, and J. Xia, 1999, Multichannel analysis of surface waves: Geophysics, **64**, 800–808, https://doi.org/10.1190/1.1444590.

Pérez Solano, C. A., D. Donno, and H. Chauris, 2014, Alternative waveform inversion for surface wave analysis in 2-D media: Geophysical Journal International, **198**, 1359–1372, https://doi.org/10.1093/gji/ggu211.

Shi, T., J. Zhang, Z. Huang, and C. Jin, 2015, A layer-stripping method for 3D near-surface velocity model building using seismic first-arrival times: Journal of Earth Science, **26**, 502–507, https://doi.org/10.1007/s12583-015-0569-0.

Sirgue, L., and R. G. Pratt, 2004, Efficient waveform inversion and imaging: A strategy for selecting temporal frequencies: Geophysics, **69**, 231–248, https://doi.org/10.1190/1.1649391.

Xia, J., R. D. Miller, and C. B. Park, 1999, Estimation of near-surface shear-wave velocity by inversion of Rayleigh waves: Geophysics, **64**, 691–700, https://doi.org/10.1190/1.1444578.

Xia, J., R. D. Miller, C. B. Park, and G. Tian, 2002, Determining Q of near-surface materials from Rayleigh waves: Journal of Applied Geophysics, **51**, 121–129, https://doi.org/10.1016/S0926-9851(02)00228-8.

Yilmaz, Ö., 2015, Engineering seismology with applications to geotechnical engineering: SEG.